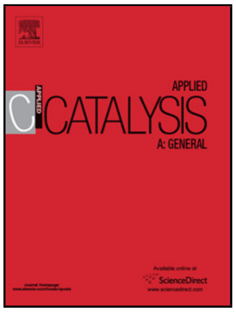

Title: Three-dimensional<!–<query id="Q2">Please check the presentation of the article title, and amend if necessary.</query>–> ordered mesoporous Ce$_x$Zr$_{1-x}$O$_2$ for selective catalytic reduction removal of NO$_X$ with NH$_3$

Author: Yi Li Yuan Wan Yanping Li Sihui Zhan Qingxin Guan Yang Tian

PII: S0926-860X(16)30485-9
DOI: http://dx.doi.org/doi:10.1016/j.apcata.2016.10.001
Reference: APCATA 16017

To appear in: *Applied Catalysis A: General*

Received date: 24-7-2016
Revised date: 25-9-2016
Accepted date: 3-10-2016

Please cite this article as: Yi Li, Yuan Wan, Yanping Li, Sihui Zhan, Qingxin Guan, Yang Tian, Three-dimensional ordered mesoporous CexZr1−xO2 for selective catalytic reduction removal of NOX with NH3, Applied Catalysis A, General http://dx.doi.org/10.1016/j.apcata.2016.10.001

<AT>Three-Dimensional Ordered Mesoporous $Ce_xZr_{1-x}O_2$ for Selective Catalytic Reduction Removal of NO_X with NH_3

<AU>Yi Li[a], Yuan Wan[a], Yanping Li[a], Sihui Zhan[b*]
##Email##sihuizhan@nankai.edu.cn##/Email##, Qingxin Guan[b], Yang Tian[c]
<AU>
<AFF>[a]Department of Chemistry, Tianjin University, Tianjin 300072, PR China
<AFF>[b]College of Environmental Science and Engineering, Nankai University, Tianjin 300071, PR China
<AFF>[c]Department of Chemistry, Capital Normal University, Beijing 100875, PR China
<PA>Tel.: /Fax: +86-22-23501117.

<ABS-HEAD>Highlights► Highly ordered mesoporous $Ce_xZr_{1-x}O_2$ have been fabricated for NH_3-SCR of NO using KIT-6 as a hard template ► The sample shows superior composite crystal microstructure, uniform mesopore diameter and larger surface area ► The mesoporous $Ce_{0.67}Zr_{0.33}O_2$ shows the best NH_3-SCR activity to clean NO_X

<ABS-HEAD>Abstract

<ABS-P>A series of highly ordered mesoporous $Ce_xZr_{1-x}O_2$ (x represents the mole ratio of Ce), were fabricated for NH_3-SCR of NO_X using KIT-6 as a hard template, which have been characterized by TEM, XRD, BET, BJH, XPS, H_2-TPR, NH_3-TPD and in-situ DRIFT, showing superior composite crystal microstructure, uniform mesopore diameter and larger surface area. Among all the mesoporous $Ce_xZr_{1-x}O_2$ samples (x=0, 0.25, 0.33, 0.5, 0.67, 0.75 and 1), mesoporous $Ce_{0.67}Zr_{0.33}O_2$ showed the best NH_3-SCR activity to clean NO_X, and 100% NO_X conversion ratio at 325°C can be reached, as well as excellent H_2O or SO_2 tolerance and best thermal stability. Furthermore, the addition of ZrO_2 content enhanced the thermal performance and redox ability of mesoporous $Ce_xZr_{1-x}O_2$, which were favorable for their excellent NH_3-SCR performance. Finally, a possible redox reaction mechanism of NH_3-SCR reaction over the mesoporous $Ce_xZr_{1-x}O_2$ was proposed.

<KWD>Keywords: mesoporous $Ce_xZr_{1-x}O_2$; NH_3-SCR; H_2O or SO_2 durability; reaction mechanism.

<H1>1. 1
Introduction

Nitrogen oxides (NO_X) from vehicle exhaust gas or fossil fuels have always been a major air pollutant in recent years, which are harmful to the health of human beings, resulting in acid rain, photochemical smog, ozone depletion and greenhouse effects.[1-2] Currently, selective catalytic reduction (SCR) technology remains as the most attractive and widely-used method to reduce NO_X, which has a large choice of reductants such as alcohol, ammonia, hydrocarbons, urea, hydrogen, etc.[3-6] As we all know, NH_3-SCR is demonstrated as one of the most widely-used and high-effective approaches.[7] The most widely used commercial catalyst for the NH_3-SCR process is V_2O_5-WO_3/TiO_2 in a temperature range of 300-400 °C. However, V_2O_5-WO_3/TiO_2 catalyst has many drawbacks such as toxicity of vanadium, SO_2 poisoning phenomenon and narrow temperature window [8] Owing to these disadvantages, many researchers have done a lot of effort to develop novel SCR catalyst with excellent performance, nontoxicity to the environment, wide operating window and excellent H_2O or SO_2 tolerance.

As the most abundant rare earth oxide, cerium oxide (CeO_2) possesses a high catalytic performance in many fields such as water-gas shift, carbon monoxide oxidation and reforming reaction.[9] In addition, CeO_2 has good redox properties, however, its high temperature sintering leading to the ceria inactive for the redox reaction of Ce^{4+} to Ce^{3+}.[9] Therefore its thermal stability in catalytic process should be increased.[10] It has been reported that the thermal stability can be improved when ZrO_2 joined.[11] It is said that Zr incorporation into the Ce lattice forms a ceria-zirconia solid solution.[9] Also the incorporation of Zr^{4+} into CeO_2 crystal lattice brings about a great increase in the reducibility of Ce^{4+} to Ce^{3+}.[9] That is to say, Ce-Zr mixed oxides not only possess the oxygen storage capacity of CeO_2 but also have the highly thermal performance of ZrO_2, which is considered as a feasible approach to overcome the aforementioned disadvantages of pure CeO_2.[12-13] However, amorphous materials can agglomerate easily, resulting in the decline of NH_3 adsorption ability during the catalytic process.[14] To address the above problem, the material with controllable structures, sizes, and shapes have been extensively investigated as potential catalyst because of their abundant active sites, large specific surface areas and interconnected channels.[15-16] To our knowledge, mesoporous materials with well-defined pore diameters and large surface areas in SCR process have drawn much attentions in recent years,[18-21] such as mesoporous Co_3O_4[22], mesoporous $MnCo_2O_4$[14], etc. Meoporous Ce-Zr composite oxides for SCR removal of NO_X with NH_3 is not reported until now. Herein, highly ordered mesoporous $Ce_xZr_{1-x}O_2$, were fabricated for NH_3-SCR of NO_X by using KIT-6 as a hard template, which contained very good composite crystal structure, uniform size and larger surface area. The highly ordered mesoporous materials then characterized by TEM, XRD, NH_3-TPD, H_2-TPR, XPS, BET and in-situ DRIFT. Compared with bulk Ce-Zr mixed oxide nanoparticles, mesoporous $Ce_xZr_{1-x}O_2$ showed better SCR removal activity and SO_2, H_2O resistance. Finally, a redox reaction mechanism with the mesoporous $Ce_xZr_{1-x}O_2$ was proposed.

<H1>2. Experimental

<H2>2.1 Preparation of materials

The 3D mesoporous $Ce_xZr_{1-x}O_2$ catalyst, with a Ce/Zr molar ratio of 2:1, was prepared via hard template synthesis method. 5.6449 g of $Ce(NO_3)_3 \cdot 6H_2O$ and 1.6186 g of $ZrO(NO_3)_2$ were added into 30 mL deionized water. After the mixed solution was dissolved completely, 2.4212 g of KIT-6 sample was added to the above solution at room temperature. Before the above samples were dried at 80 °C for 4 h, the mixtures were stirred at room temperature for 24 hours followed by calcination at 500 °C for 6 h in the air atmosphere in a muffle furnace with a heating rate of 1 °C/min. After cooling to room temperature, the samples were available in powders. Finally, the obtained powders were washed in 2 mol/L NaOH aqueous solution for twice then washed in deionized water several times until pH=7 and dried at 60 °C in the oven. The synthesis processes of other mesoporous $Ce_xZr_{1-x}O_2$ (x represented the Ce molar ratio. x=0, 0.25, 0.33, 0.5, 0.67, 0.75 and 1) samples were similar with the above steps. The sample of $Ce_{0.67}Zr_{0.33}O_2$ without mesoporous structure is denoted as bulk $Ce_{0.67}Zr_{0.33}O_2$. The preparation process was almost similar with mesoporous $Ce_{0.67}Zr_{0.33}O_2$ and the main difference was no KIT-6 adding into the mixture.

The synthetic strategy is schematically illustrated in Fig. 1. In brief, cubic phase KIT-6 was first prepared based on previous published paper.[23-24] Then KIT-6 was added to the $Ce_xZr_{1-x}O_2$ precursors, then both the template and precursors were stirred with each other under magnetic stirring for 24 h. Mesoporous $Ce_xZr_{1-x}O_2$ were obtained after removing the porous silica template.

<H2>2.2 Characterization

Transmission electron microscopy (TEM, JEOL JEM-2100F with an accelerating voltage of 200 kV, Japan) was used to characterize the size and morphology of the mesoporous $Ce_xZr_{1-x}O_2$. X-ray diffraction (XRD Rigaku D/Max 2200PC, Japan) patterns were performed employing a CuKα radiation (λ=0.15418 nm, 40 kV, 40 mA) at room temperature. The nitrogen adsorption-desorption isotherms were measured by ASAP Autosorb iQ-MP instrument operated at -196 °C. Characterization of the surface area of the samples was obtained with the Brunauer-Emmett-Teller (BET) method, and the pore size distributions of the samples were recorded with the adsorption branches and a cylindrical pore model (BJH method). The data of the binding energies of Ce 3d, Zr 3d and O 1s were obtained by XPS (Thermal ESCALAB 250) with an AlKα radiation X-ray source (hν=1486.6 eV) referencing the C 1s peak at 284.6 eV. Temperature-programmed reduction by hydrogen (H_2-TPR) and temperature-programmed desorption of NH_3 (NH_3-TPD) were tested by a Micromeritics Autochem 2920 II instrument with a thermal conductivity detector (TCD). Visible Raman spectra of the catalysts were collected in Via Raman microscope (Renishaw) with a spectral resolution of 1.14 cm^{-1} at room temperature. A 514 nm diode-pumped solid-state semiconductor laser was used as the excitation source. A FTIR spectrometer (Thermo Nicolet iS5) equipped with a liquid-nitrogen-cooled MCT detector was used to collect the in-situ DRIFT data.

<H2>2.3. Catalytic Performance Tests

The activity measurements were tested in a fixed-bed quartz reactor with an i.d. of 10 mm and operated under atmospheric pressure in a temperature window from 150 to 450 °C. 0.2 g of catalysts was used, which was crushed and sieved to 40-60 mesh. The test conditions contained 500 ppm NO, 500 ppm NH_3, 3% O_2, 100 ppm or 200 ppm SO_2 and 5% or 10% H_2O (when used), which were balanced by N_2 with a gas hourly space velocity of 9.0×10^4 h^{-1} and a flow rate of 200 mL/min. What's more, the gas-phase concentrations of all components were measured using a KM-940 flue gas analyzer from Kane International Limited in UK. The detailed analysis method in KM-940 is electro-chemical principle. Firstly, the sensor in KM-940 has a self-test process. Then, the reaction gases NO_X, NH_3 and O_2 from different pipelines are well mixed by gas mixer. The mixes enter into the reactor and have the NH_3-SCR reaction under the mesoporous $Ce_xZr_{1-x}O_2$ catalyst. After the reaction, gases get into the sensor by the suction pump. According to a signal conversion in sensor, the remaining content of the gases (NO, NO_2, N_2O) are showed on KM-940's monitor. Based on these data, we can finally work out the NO_X conversion rate. The formula below ($[NO_X]_{in}$ was inlet NO_X concentration and $[NO_X]_{out}$ was outlet NO_X concentration, respectively), the NO_X conversion ratio and N_2 selectivity under steady-state reaction condition was tested.

$$NO_X\ conversion\ (\%) = 100\%\ \times (1 - [NO_X]_{out}/[NO_X]_{in})$$

$$N_2\ selectivity\ (\%) = 100\%\ \times \{1 - \frac{([NO_2]_{out} + 2[N_2O]_{out})}{([NO_X]_{in} + [NH_3]_{in} - [NO_X]_{out} - [NH_3]_{out})}\}$$

<H1>3. Results and discussion

<H2>3.1 NH_3-SCR Activity

NH_3-SCR performances of mesoporous Ce-Zr samples were measured as a function of temperature with a gas hourly space velocity of 9.0×10^4 h^{-1} and the results are shown in Fig. 2a. The different mesoporous $Ce_xZr_{1-x}O_2$ samples show good catalytic activities，which can be reached more than 90% conversion ratio in a large temperature window between 250-325 °C. What's more, for mesoporous $Ce_{0.67}Zr_{0.33}O_2$, the SCR activity achieves more than 95% NO_X conversion ratio between 250-375 °C, which is enhanced to nearly 100% at 325 °C. However, the best NO_X conversion ratios for pure CeO_2 and ZrO_2 can only reach 80% and 30%, respectively. It can be concluded that NO_X conversion ratios with mesoporous $Ce_xZr_{1-x}O_2$ materials are much higher than that of single metal oxide in the whole temperature window. In addition, the SCR removal activity of mesoporous $Ce_{0.67}Zr_{0.33}O_2$ is slightly higher than mesoporous $Ce_{0.75}Zr_{0.25}O_2$, $Ce_{0.5}Zr_{0.5}O_2$, $Ce_{0.33}Zr_{0.67}O_2$ and $Ce_{0.25}Zr_{0.75}O_2$, indicating a zirconium limit of the synergistic effect between Ce-Zr. In order to compare with mesoporous Ce-Zr sample, a conventional V_2O_5-WO_3/TiO_2 and bulk $Ce_{0.67}Zr_{0.33}O_2$ are also performed in Fig. 2b. As shown in Fig. 2b, the SCR performance over VWTi catalyst can only reach 90% at 225-250 °C, which is a narrow temperature window. Then, it decrease quickly to less than 80% above 275 °C. The NO_X conversion ratio over mesoporous $Ce_{0.67}Zr_{0.33}O_2$ is much better than commercial VWTi in a wide temperature window of 200-400 °C, which can achieve more than 95% NO_X conversion ratio in such a wide temperature window of 250-375 °C. On the contrary, mesoporous $Ce_{0.67}Zr_{0.33}O_2$ also exhibits a better NH_3-SCR ability than bulk $Ce_{0.67}Zr_{0.33}O_2$ in the whole temperature windows. As previous literatures described,[18-20] mesoporous structures with better dispersion of active Ce-Zr components play an important role in NH_3-SCR reactions. In addition, the following TEM pictures, low-angle and wide-angle XRD patterns and N_2 adsorption-desorption isotherms of $Ce_xZr_{1-x}O_2$ samples demonstrate the existence of highly unified meso-pores with large specific surface area and good dispersion in $Ce_xZr_{1-x}O_2$ catalyst. Great mass transfer ability and more exposed active sites brought by the uniform active channels make a significant contribution to the interaction between Ce-Zr species, hence resulting in the excellent catalytic activity. The N_2 selectivity was also tested for the mesoporous and bulk $Ce_{0.67}Zr_{0.33}O_2$ as shown in Fig. 2b (inset). The two samples keep close to 100% N_2 selectivity during the temperature range 50-350 ˚C which started to decrease at about 400 ˚C and down to 79.4% and 70.1% at 450 ˚C, respectively, indicating that the synergistic effect between Ce-Zr elements can significantly improve the selectivity. As we all know, GHSV is another influential factor needed to be considered in the SCR process, which is influenced by its weight as well as gas flow rate. The SCR performance over mesoporous/bulk $Ce_{0.67}Zr_{0.33}O_2$ and V_2O_5-WO_3/TiO_2 under different GHSVs of 30000, 90000 and 180000 h^{-1} have been tested as shown in Fig. 2c-e. For mesoporous $Ce_{0.67}Zr_{0.33}O_2$, it can be observed that the NO_X removal ratio decreases slightly with increasing GHSVs from 30000 to 180000 h^{-1} due to a shorter contact time between the catalyst and the mixed gases in Figure 2c.[25] Overall the GHSV has little influence on the SCR activity in the entire temperature windows. The mesoporous $Ce_{0.67}Zr_{0.33}O_2$ still reaches more than 98% at temperatures ranging from 250 to 350 °C with a GHSV of 30000 h^{-1}. Even at a high GHSV of 180000 h^{-1}, the NO_X conversion ratio achieves nearly 95% at a temperature window of 250-325 °C. However, the NO_X conversion ratio over bulk $Ce_{0.67}Zr_{0.33}O_2$ in Figure 2d has a relatively clear difference under GHSVs of 30000, 90000 and 180000 h^{-1}. There obtain 78-85% NO_X conversion ratios at a temperature window of 250-350 °C with a GHSV of 30000 h^{-1} while 68-70% NO_X conversion ratios with a GHSV of 180000 h^{-1}. In addition, the trends under different GHSVs over commercial VWTi seem to be more clearly in Figure 2e. The NO_X conversion ratios exit an apparent decline when the GHSV rose from 30000 to 180000 h^{-1} in the whole temperature window. In general, mesoporous $Ce_{0.67}Zr_{0.33}O_2$ does better in NH_3-SCR under different GHSVs than bulk $Ce_{0.67}Zr_{0.33}O_2$ and V_2O_5-WO_3/TiO_2.

<H2>3.2 Characterizations of catalyst

Prior to the investigations of mesoporous $Ce_xZr_{1-x}O_2$ in NH_3-SCR activities, the internal construction of the samples were systematically observed via TEM. The results are illustrated in Fig. 3 and Fig. S1. The sample of $Ce_xZr_{1-x}O_2$ presents arrays of three dimensional high-ordered mesoporous structures, guaranteeing a large specific surface area to enhance the NH_3 adsorption capacity. Moreover, Fig. 3c shows the picture of bulk $Ce_{0.67}Zr_{0.33}O_2$, which doesn't have any mesoporous structure in the whole horizon. Compared to the results in Fig. 3 (a, b, d) and Fig. S1, more zirconium doped contents result in worse regulation of mesoporous channels, which are in agreement with the result of low-angle XRD patterns. Moreover, high-resolution transmission electron microscopy (HRTEM) was used to characterize the lattice structure of 3D mesoporous $Ce_{0.67}Zr_{0.33}O_2$. As shown in Fig. 3e, two different lattice fringes can be clearly observed in vision. One is around 0.314 nm, matching well with CeO_2 in plane (110) [26-27] and another one is 0.298 nm, corresponding to ZrO_2 in plane (101).[28-29] Meanwhile, energy dispersive X-ray spectroscopy (EDS) was also used to explore the chemical composition of the mesoporous $Ce_{0.67}Zr_{0.33}O_2$ (Fig. 3f). It clearly certifies that the material is made up of Ce, Zr and O elements, which perfectly agrees with the theoretical value. By the way, the existence of C and Cu peak in EDS spectrum maybe come from the copper mesh used in TEM tests.

In order to study the mesoporous structure and crystalline nature $Ce_xZr_{1-x}O_2$ in detail, low-angle and wide-angle XRD patterns were confirmed in Fig. 4. As shown in Fig. 4a, the characteristic reflection peaks at approximately 1.1° and 1.9° for mesoporous $Ce_{0.67}Zr_{0.33}O_2$ are revealed, indicating a highly ordered mesostructure.[14] Notably, it is clear that the well-defined peaks corresponded to 1.2° and 2.0° are observed in pure CeO_2, also exhibiting the existence of well-ordered mesoporous structures, which is in agreement with the TEM image showed in Fig. S1g. However, pure ZrO_2 has weak peaks in low-angle XRD patterns, suggesting relative poor orderliness. Moreover, the low-angle patterns of different mesoporous Ce-Zr samples are also showed in Fig. 4a, it can be found that there is no clear difference between $Ce_{0.75}Zr_{0.25}O_2$, $Ce_{0.67}Zr_{0.33}O_2$ and $Ce_{0.5}Zr_{0.5}O_2$ whereas the peaks of these three samples are stronger than that of $Ce_{0.33}Zr_{0.67}O_2$ and $Ce_{0.25}Zr_{0.75}O_2$, testifying more zirconium contents result in worse regulation of mesoporous channels, which are in agreement with TEM results. Wide angle XRD patterns of $Ce_xZr_{1-x}O_2$ are shown in Fig. 4b. The characteristic reflections of mesoporous $Ce_xZr_{1-x}O_2$ at $2\theta = 28.87°$, 33.47°, 48.05°, 57.01° and 59.85°, corresponding to the (1 1 1), (2 0 0), (2 2 0), (3 1 1) and (2 2 2) phases respectively, which can be well indexed to CeO_2 (JCPD 81-0792). Similarly, the characteristic reflections at 2θ =28.6°, 30.27°, 34.81°, 50.71° and 60.21°, which are responsible for (0 1 1), (0 0 2), (0 2 0), (3 1 1) and (1 2 1) planes of ZrO_2 (JCPD 50-1089), respectively. In addition, the addition of ceria to $Ce_xZr_{1-x}O_2$ leads to a slightly shift of XRD peaks to higher values.[12] And noteworthy, the peak intensity belonging to zirconium species are weakened in $Ce_xZr_{1-x}O_2$ samples, suggesting an appropriate synergistic reaction between Ce-Zr.

The N_2 adsorption-desorption isotherms and pore diameter distributions of mesoporous $Ce_XZr_{1-X}O_2$ and bulk $Ce_{0.67}Zr_{0.33}O_2$ are shown in Fig. 5. As presented in picture, the curves of mesoporous $Ce_{0.67}Zr_{0.33}O_2$, CeO_2, ZrO_2 in Fig. 5a and mesoporous $Ce_{0.75}Zr_{0.25}O_2$, $Ce_{0.5}Zr_{0.5}O_2$, $Ce_{0.33}Zr_{0.67}O_2$, $Ce_{0.25}Zr_{0.75}O_2$ in Fig. 5b are verified as type IV isotherms with type H1 hysteresis loops, indicating the typical characters of mesoporous metal oxides replicated from KIT-6.[30-32] However, the bulk $Ce_{0.67}Zr_{0.33}O_2$ does not exhibit the typical IV type isotherm, suggesting that the bulk $Ce_{0.67}Zr_{0.33}O_2$ has not mesoporous channels. Based on the data shown in Fig. 5c-d, it can be concluded that the pore size distributions of all mesoporous samples are similar, which exist a peak value near 5-5.5 nm. However, the average pore size of bulk $Ce_{0.67}Zr_{0.33}O_2$ causes a left-shift to near 4 nm. Meanwhile, the data of specific surface areas and pore volumes are listed in Table 1. As shown in Table 1, mesoporous $Ce_{0.75}Zr_{0.25}O_2$ (118.8 m^2/g), mesoporous $Ce_{0.67}Zr_{0.33}O_2$ (118.3 m^2/g) and mesoporous $Ce_{0.5}Zr_{0.5}O_2$ (110.1 m^2/g) have relatively bigger surface area of exceeding 110 m^2/g and pore volume of 0.34, 0.35 and 0.29 cm^3/g respectively, which are much larger than mesoporous $Ce_{0.33}Zr_{0.67}O_2$, mesoporous $Ce_{0.25}Zr_{0.75}O_2$, mesoporous CeO_2, mesoporous ZrO_2 and bulk $Ce_{0.67}Zr_{0.33}O_2$ with surface areas of 88.5, 79.4, 28.7, 15.8 and 68.9 m^2/g and pore volumes of 0.23, 0.22, 0.16, 0.12 and 0.21 cm^3/g, respectively. A larger specific surface area always represents a larger NH_3 adsorption capacity. In conclusion, it is suggested that the reduction activity of NO_X in NH_3-SCR is related to the apparent surface properties to some extent.

XPS measurements of Ce 3d, Zr 3d, O 1s of Ce-Zr samples were carried out to investigate the surface states. As shown in Fig. 6a, the series of v and u peaks in Ce 3d core-level spectra are from the 3d5/2 and 3d3/2 states, respectively. XPS peaks labeled as v (883.3 eV), v'' (889.7 eV), v''' (898.5 eV), u (902.0 eV), u'' (908.4 eV), and u''' (917.6 eV) correspond to the $3d^{10}4f^0$ state of Ce^{4+} species, whereas the peaks signed as v' (885.1 eV) and u' (903.5 eV) are assigned to the $3d^{10}4f^1$ state of Ce^{3+}.[33-34] The Zr 3d core level spectrum in Fig. 6b-c display two peaks approximately at 182.8 eV and 185.3 eV, assigned to the Zr 3d5/2 and Zr 3d3/2 spin-orbit states, respectively.[35] Furthermore, the surface atom concentrations of Ce, Zr and O of mesoporous $Ce_XZr_{1-X}O_2$ and bulk $Ce_{0.67}Zr_{0.33}O_2$ are summarized in Table 2. The percent of O on mesoporous $Ce_{0.75}Zr_{0.25}O_2$ and $Ce_{0.67}Zr_{0.33}O_2$ clearly achieve 89.69% and 89.99%, which are higher than CeO_2, ZrO_2 and bulk $Ce_{0.67}Zr_{0.33}O_2$. Moreover, the percent of O on other mesoporous samples such as $Ce_{0.5}Zr_{0.5}O_2$ (88.83%), $Ce_{0.33}Zr_{0.67}O_2$ (87.55%) and $Ce_{0.25}Zr_{0.75}O_2$ (86.90%) also show better results than single metal oxides, that's why the composite catalysts are superior to single catalysts. In addition, the peaks of O 1s are observed in the XPS spectrum, as shown in Fig. 6d-e. The O 1s spectrum can be fitted into two peaks, which correspond to various oxygen containing chemical bonds.[36] The binding energy approximately at 529.8 eV corresponds to lattice oxygen O^{2-}, which is denoted as the surface lattice oxygen O_β. And O^-, which has a higher binding energy approximately at 531.8 eV, is denoted as the surface chemisorbed oxygen O_α.[35] As is well-known, the surface chemisorbed oxygen acts as the most active oxygen and plays an indispensable role in oxidation reactions.[37] The ratio of $O_\alpha/(O_\alpha+O_\beta)$ in mesoporous samples are much higher than that in mesoporous CeO_2 (43.35%) and ZrO_2 (24.69%), which may be due to the interaction between the zirconium and cerium oxides. Moreover, the ratio of $O_\alpha/(O_\alpha+O_\beta)$ in mesoporous $Ce_{0.67}Zr_{0.33}O_2$ (58.48%) is also much higher than that in bulk $Ce_{0.67}Zr_{0.33}O_2$ (45.19%), suggesting the mesoporous structure promises more generation of surface chemisorbed oxygen than bulk sample in NH_3-SCR. In addition, there exist slight differences between mesoporous $Ce_XZr_{1-X}O_2$ samples. The ratio of $O_\alpha/(O_\alpha+O_\beta)$ follow the sequence of mesoporous $Ce_{0.75}Zr_{0.25}O_2$ > mesoporous $Ce_{0.67}Zr_{0.33}O_2$ > mesoporous $Ce_{0.5}Zr_{0.5}O_2$ > mesoporous $Ce_{0.33}Zr_{0.67}O_2$ > mesoporous $Ce_{0.25}Zr_{0.75}O_2$, which are accorded with the NH_3-SCR activity on the whole shown in Fig. 2, except for a slight inconformity between mesoporous $Ce_{0.75}Zr_{0.25}O_2$ and mesoporous $Ce_{0.67}Zr_{0.33}O_2$ results. That's because the ratio of $O_\alpha/(O_\alpha+O_\beta)$ is a significant NH_3-SCR influencing factor but not the only element in NH_3-SCR process. The XPS spectra of Ce 3d, Zr 3d, and O 1s of mesoporous $Ce_XZr_{1-X}O_2$ and bulk $Ce_{0.67}Zr_{0.33}O_2$ are shown in Fig. 6f, these kinds of absorbed peaks were calibrated against the C 1s peak standardized at 284.6 eV.

H_2-TPR experiments were conducted to investigate the redox abilities of catalysts, and the results are shown in Fig. 7a. It is clear that the H_2 consumption peaks over the four samples are generally located at 150-500 and 500-700 °C, attributed to the surface lattice oxygen and bulk lattice oxygen, respectively.[38] Based on the whole reduction process, the surface lattice oxygen promotes the reduction of Ce^{4+} to Ce^{3+} via oxygen vacancy generation, then the oxygen vacancy oxygen progressively triggers the bulk lattice oxygen to complete the reduction process of Ce^{4+} to Ce^{3+}.[38] As shown in Fig. 7a, the reduction peak at 406 °C in mesoporous $Ce_{0.67}Zr_{0.33}O_2$ assigned to surface lattice oxygen moves to higher temperature at 423 °C and has weaker peak intensity in mesoporous CeO_2, suggesting the mesoporous $Ce_{0.67}Zr_{0.33}O_2$ has more available surface lattice oxygen at lower temperature after the introduction of zirconium.[39] The peak located in 475 °C has a relatively high intensity, which is assigned to the surface lattice oxygen in ZrO_2. Moreover, the reduction peaks at 262 °C and 406 °C in mesoporous $Ce_{0.67}Zr_{0.33}O_2$ are observed in lower temperature and have stronger peak intensities than bulk $Ce_{0.67}Zr_{0.33}O_2$ at 294 °C and 460 °C, indicating the mesoporous structure has a stronger synergetic effect among Ce and Zr.[40] The intensity trend attributed to the bulk lattice oxygen is a little different with the surface lattice oxygen, following the sequence of mesoporous CeO_2 > mesoporous $Ce_{0.67}Zr_{0.33}O_2$ > bulk $Ce_{0.67}Zr_{0.33}O_2$. It may owe to the fact that part of bulk lattice oxygen translates into surface lattice oxygen in $Ce_{0.67}Zr_{0.33}O_2$ samples after the introduction of Zr content.[12] In addition, other mesoporous $Ce_xZr_{1-x}O_2$ (x=0.75, 0.5, 0.33, 0.25) samples were also tested for comparison as shown in Fig. 7b. Compared to mesoporous $Ce_{0.67}Zr_{0.33}O_2$, the reduction peak at 493 °C and 692 °C in mesoporous $Ce_{0.75}Zr_{0.25}O_2$ assigned to surface lattice oxygen and bulk lattice oxygen move to higher temperature, suggesting the higher temperature of available oxygen in mesoporous $Ce_{0.75}Zr_{0.25}O_2$. Also, the peak located in 493 °C and 686 °C of mesoporous $Ce_{0.5}Zr_{0.5}O_2$ have a bit weaker peak intensity than mesoporous $Ce_{0.75}Zr_{0.25}O_2$ and $Ce_{0.67}Zr_{0.33}O_2$, which suggests that more Ce species can enhance the catalyst activity.

With more introduction of zirconium, clear intensity decreases can be seen in mesoporous $Ce_{0.33}Zr_{0.67}O_2$ (403 °C and 511 °C) and mesoporous $Ce_{0.25}Zr_{0.75}O_2$ (410 °C and 700 °C), which agree with the NH_3-SCR performance.

NH_3-TPD was carried out to investigate the surface acid amount and acid strength of catalyst because the adsorptions and activations of NH_3 on active sites of catalyst surface possess significant effects on NH_3-SCR. As shown in Fig. 7c, the profiles exhibit two distinct desorption peaks, suggesting two kinds of acid sites on the surface of the samples. Desorption peaks located at low temperature (lower than 400 °C) are assigned to the weak and medium acid sites on the catalysts surface, which is attributed to the Brønsted acid sites. While desorption peaks centered at high temperature (higher than 600 °C) are assigned to the strong acid sites, which is originated from the Lewis acid sites.[37] Based on previous literature,[39] the absorbed NH_3 is related to the weaker acid sites, indicating Brønsted acid sites act as a predominant role in the NH_3-SCR. As seen in Fig. 7c, the corresponding desorption strength follow sequence of mesoporous $Ce_{0.67}Zr_{0.33}O_2$ > bulk $Ce_{0.67}Zr_{0.33}O_2$ > mesoporous CeO_2 > mesoporous ZrO_2, which are accorded with the NH_3-SCR activity shown in Fig. 2. Mesoporous $Ce_{0.67}Zr_{0.33}O_2$ exhibits much more Lewis acid sites and Brønsted acid sites than other samples, leading to a remarkable improvement of NH_3 adsorption and activation SCR process.[41] Moreover, other mesoporous $Ce_xZr_{1-x}O_2$ (x=0.75, 0.5, 0.33, 0.25) samples were also tested for comparison as shown in Fig. 7d. Expect for a small peak shifting, the strong peak trends in mesoporous $Ce_{0.75}Zr_{0.25}O_2$ (250 °C, 401 °C and 632 °C) and $Ce_{0.5}Zr_{0.5}O_2$ (209 °C, 354 °C and 538 °C) are as similar with mesoporous $Ce_{0.67}Zr_{0.33}O_2$, indicating relatively good NH_3-SCR performance with these three samples. However, the peaks with mesoporous $Ce_{0.33}Zr_{0.67}O_2$ (385 °C and 501 °C) and $Ce_{0.25}Zr_{0.75}O_2$ (233 °C and 450 °C) have clear decreases in peak intensity, which demonstrates weaker surface acid amount adsorptions and acid strengths of catalysts. These appearances conform to the SCR results as shown above.

As shown in Fig. 8, visible Raman spectra were also used to characterize the constituent of samples. The Ce content samples show a clear band at 463 cm^{-1}, suggesting the Raman-active F_{2g} mode of the CeO_2.[12] The band at 271 cm^{-1} is attributed to a consequence of the Zr phase (t-ZrO_2).[12, 42] As it can be seen, the peaks are quite similar and are characterized by a strong absorption band at 463 cm^{-1} between mesoporous $Ce_XZ_{1-X}O_2$ and bulk $Ce_{0.67}Zr_{0.33}O_2$. Pure CeO_2 and ZrO_2 present the absorption bands approximately at 463 cm^{-1} and 271 cm^{-1}, respectively. Based on current literatures, there should exit a band approximately at 630 cm^{-1} assigned to the lattice contraction caused by Zr ion insertion, which is not obviously in $Ce_{0.67}Zr_{0.33}O_2$ samples and especially in pure ZrO_2.[43]

<H2>3.3 The resistance of H_2O or SO_2, and thermal stability tests

In practical application, the existence of H_2O vapor and SO_2 in the combustion exhaust may lead to deactivation of the performance of SCR.[44] Hence, it is necessary to investigate the influence of H_2O and SO_2 on catalytic performance in NH_3-SCR process. In this paper, 10%, 15% H_2O and 100 ppm of SO_2 over mesoporous $Ce_{0.67}Zr_{0.33}O_2$ were tested at 300 °C under a GHSV of 90000 h^{-1}. As a comparison, widely-used commercial V_2O_5-WO_3/TiO_2 and bulk $Ce_{0.67}Zr_{0.33}O_2$ were also measured in 10%, 15% H_2O and 100 ppm of SO_2. As shown in Fig.

9a, the NO_X conversion ratio of mesoporous $Ce_{0.67}Zr_{0.33}O_2$ decreases from 98% to 95% in the absence of 10% H_2O at 300 °C and then maintains this state in consecutive testing process for the next 40 h. A rapidly recovery to the original level of 98% NO_X conversion is found when cutting off the introduction H_2O. V_2O_5-WO_3/TiO_2 displays a stable 91% NO_X conversion ratio at 300°C and decreases to 85% in the absence of 10% H_2O, then recovers to 90% NO_X conversion when cutting off the introduction H_2O. The NO_X conversion ratio of bulk $Ce_{0.67}Zr_{0.33}O_2$ decreases from 81% to 74% in the absence of 10% H_2O then recovers to the original level slowly. In addition, the injection of 15% H_2O into the reaction atmosphere leads to a slight decrease from 98% to 93% during the whole testing for mesoporous $Ce_{0.67}Zr_{0.33}O_2$, which also showed a recovery to its original level after cutting off the inlet H_2O (Fig. 9b). Commercial V_2O_5-WO_3/TiO_2 falls to 80% in the 15% H_2O reaction atmosphere and recovers to 90% when turning off the H_2O entrance. The NO_X conversion ratio of bulk $Ce_{0.67}Zr_{0.33}O_2$ decreases from 81% to 69% in the absence of 15% H_2O, which recovers to the original level slowly. It is believed that a competition adsorption exists between H_2O and NH_3/ NO_X on the catalyst surface. H_2O occupies the active sites where the NH_3/ NO_X activated, resulting in a decline in NH_3-SCR.[12] The results indicate that mesoporous $Ce_{0.67}Zr_{0.33}O_2$ shows a better H_2O resistance ability in NH_3-SCR process than that of commercial V_2O_5-WO_3/TiO_2 and bulk $Ce_{0.67}Zr_{0.33}O_2$. Moreover, the effect of SO_2 over mesoporous $Ce_{0.67}Zr_{0.33}O_2$, V_2O_5-WO_3/TiO_2 and bulk $Ce_{0.67}Zr_{0.33}O_2$ are exhibited in Fig. 9c. With the introduction of 100 ppm SO_2, the NO_X conversion ratio shows a slow decrease in the first 10 h over mesoporous $Ce_{0.67}Zr_{0.33}O_2$. Then, SO_2 poisoning occurs in mesoporous $Ce_{0.67}Zr_{0.33}O_2$, leading to a decline in the conversion ratio to 87% with the time increasing. However, after cutting off the SO_2, the conversion ratio slowly recovers to more than 90% during the measured period. As for commercial V_2O_5-WO_3/TiO_2, NO_X conversion ratio decreases seriously from 91% to 55%. After cutting off the SO_2, the conversion ratio recovers slowly to 80% with time increasing. As for the bulk $Ce_{0.67}Zr_{0.33}O_2$, the NO_X conversion ratio decreases from 81% to 73% when 100 ppm SO_2 introduced, then finally recovers to 77% after cutting off the SO_2. In conclusion, mesoporous $Ce_{0.67}Zr_{0.33}O_2$ has a better reversible inhibition effect on SO_2 than that of commercial V_2O_5-WO_3/TiO_2 and bulk $Ce_{0.67}Zr_{0.33}O_2$. In practical application, a good resistance performance to H_2O vapor and SO_2 in the NH_3-SCR process means a considerably stable ability to the deNO_X process. We tested that mesoporous $Ce_{0.67}Zr_{0.33}O_2$ shows a bit higher resistance performance against H_2O and SO_2 than V_2O_5-WO_3/TiO_2 and bulk sample at 300 °C in figure 9 (a-c). Due to the highly unified meso-pores with large specific surface area and good dispersion between Ce-Zr, mesoporous $Ce_{0.67}Zr_{0.33}O_2$ has great mass transfer ability and more exposed active sites brought by the uniform active channels. When in a H_2O vapor and SO_2 circumstance, mesoporous $Ce_{0.67}Zr_{0.33}O_2$ can reserve relatively more exposed active sites to the SCR performance than V_2O_5-WO_3/TiO_2 and bulk $Ce_{0.67}Zr_{0.33}O_2$ to some extent. As shown in Fig. 9d, the stability tests of the mesoporous $Ce_{0.67}Zr_{0.33}O_2$, V_2O_5-WO_3/TiO_2 and bulk $Ce_{0.67}Zr_{0.33}O_2$ catalysts with time on stream were examined at 300 °C under a GHSV of 90000 h^{-1}. The results do not show any decrease of the NO_X conversion and maintain a 98%, 91%, 81% NO_X removal efficiencies respectively during the continuous 60 h duration, suggesting a good stability over mesoporous $Ce_{0.67}Zr_{0.33}O_2$, V_2O_5-WO_3/TiO_2 and bulk $Ce_{0.67}Zr_{0.33}O_2$ in the whole process.

<H2>3.4 In-situ DRIFT tests

The in-situ DRIFTS texts are performed to study the adsorption behaviors of the reactant molecules on the surface of catalysts, which is considered a crucial step in NH_3-SCR system. The data of NH_3 and NO + O_2 adsorptions on mesoporous $Ce_{0.67}Zr_{0.33}O_2$ from 150-450 °C are shown in Fig. 10 a. The distinct bands are assigned to gaseous NO_2 (1645, 1628 and 1392 cm^{-1}),[17, 45] bridging nitrates (1230 and 1217 cm^{-1}),[17] monodentate nitrates (1265 cm^{-1}),[38] bidentate nitrates (1600 and 1580 cm^{-1}) [12] and linear nitrites (1480 and 1410 cm^{-1}).[45] As seen, the adsorption peak intensities assign to bidentate nitrates, monodentate nitrates and gaseous NO_2 strengthen soon when the temperature increases from 150 °C to 250 °C and almost keep unchanged in 250-350 °C while show downtrend after the temperature rising to 400-450 °C. It is indicated that the three formed intermediate products during the SCR reaction on mesoporous $Ce_{0.67}Zr_{0.33}O_2$ surface are very stable and activated in the temperature range of 250-350 °C, which is in agreement with SCR abilities. Interestingly, bridging nitrates vanish soon when temperature rising from 50 °C to 250 °C and appear in 400-450 °C whereas monodentate nitrates emerge just in 250-350 °C, suggesting there may exit some transformations in different nitrates compounds and monodentate nitrates are deemed as significant parts in the SCR active window at 250-350 °C.[45] The DRIFT spectra of NH_3 desorptions on mesoporous $Ce_{0.67}Zr_{0.33}O_2$ surface are shown in Fig. 10b. The broad peaks centered at 3375 and 3264 cm^{-1} are assigned to the N-H stretching modes of coordinated NH_3.[12] The bands at 1595, 1239, and 1100 cm^{-1} can be attributed to the characteristic bands of NH_3 coordinated on Lewis acid sites.[17] The bands at 1550 and 1353 cm^{-1} are also observed as symmetric and asymmetric bending vibrations of NH_4^+ species on Brønsted acid sites.[17, 45] As shown, the intensity of the bands on sample surface show a steady increase when temperature rising to 250 °C. All types of ammonia with strong stabilities can adsorb to the catalyst surface and join in the SCR process, which is accorded with NH_3-TPD results.

In-situ DRIFTS of the reaction between pre-adsorbed NH_3 and NO + O_2 at 300 °C was recorded to study the reactivity of adsorbed NH_3 species in the SCR process on mesoporous $Ce_{0.67}Zr_{0.33}O_2$ in Fig. 10c. The mesoporous $Ce_{0.67}Zr_{0.33}O_2$ is firstly purged in a flow of NH_3 for 30 min to reach the pre-adsorbed condition and then purged by helium for 30 min at 300 °C. After the introduction of NO + O_2, the broad peaks assigned to coordinated NH_3 (3375 and 3269 cm^{-1}), Lewis acid sites (1595 cm^{-1}) and Brønsted acid sites (1551 and 1353 cm^{-1}) show an apparent decrease in intensity after 1 min. All of the bands are substituted by nitrate species after 3 min and keep stable with the time increasing, suggesting the coordinated NH_3 and ionic NH_4^+ on mesoporous $Ce_{0.67}Zr_{0.33}O_2$ can act as reducing species to reduce NO_X.[8, 12] Then the order of the gas flow are subsequently reversed, the mesoporous $Ce_{0.67}Zr_{0.33}O_2$ is firstly purged in a flow of NO + O_2 for 30 minutes to reach the pre-adsorbed condition and then purged by helium for 30 min at 300 °C. The results are shown in Fig. 10d. After the introduction of NH_3, the in-situ DRIFTS spectra are mainly covered by gaseous NO_2 (1591 and 1383 cm^{-1}), bridging nitrates (1190 cm^{-1}), bidentate nitrates (1574 cm^{-1}). The bridging nitrates are greatly decreased in 5 min and disappeared in 10 min when NH_3 was introduced, nevertheless the gaseous NO_2 and bidentate nitrates do not show an obvious changes, which indicates that bridging nitrate can react with NH_3 easily.[12] Moreover, the bands assigned to the NH_3 coordinated on Lewis acid sites (1239 and 1107 cm^{-1}) and NH_4^+ species on

Brønsted acid sites (1550 cm^{-1}) are observed after 5 min. Then these peaks keep stable with the time increasing.

<H2>3.5 Reaction mechanism

As depicted in Fig. 11, the possible reaction pathway for the selective catalytic reduction of NO_X with NH_3 over mesoporous $Ce_xZr_{1-x}O_2$ is proposed. Based on in-situ DRIFT spectra, some species from nitrogen oxides are found on the catalyst surface, including gaseous NO_2, bridging nitrate, monodentate nitrates, bidentate nitrates and linear nitrites, which are regarded as intermediate products during the SCR reaction.[45] Meanwhile, reactant gas NH_3 adsorbed on Lewis acid sites to form coordinated NH_4^+ on the surface of mesoporous $Ce_xZr_{1-x}O_2$. The gaseous NO_2 originates from NO oxidation, which is in the form of surface nitrates and nitrites through NO_2 dimerization and disproportionation.[46] Then the nitrates coordinate with NH_4^+ to form NH_4NO_3 and NH_4NO_3 subsequently connects with gaseous NH_3 and finally decomposes to N_2 and H_2O with the reactions $NH_4^+ + NO_3^- \rightarrow NH_4NO_3$, $3NH_4NO_3 + 2NH_3 \rightarrow 4N_2 + 9H_2O$.[46-47] Moreover, the nitrite directly react with surface NH_4^+ to form N_2 according to reactions $NH_4^+ + NO_2^- \rightarrow NH_4NO_2$, $NH_4NO_2 \rightarrow N_2 + 2H_2O$. Generally speaking, the reaction of NO with NH_3 follows a typical SCR mechanism ($4NO + 4NH_3 + O_2 \rightarrow 4N_2 + 6H_2O$).[48] Compared to bulk $Ce_{0.67}Zr_{0.33}O_2$, mesoporous $Ce_{0.67}Zr_{0.33}O_2$ with very good composite crystal structure, uniform size and larger surface area can provide abundant contact areas for nitrogen oxides to translate into nontoxic N_2 and H_2O. Similarly, there also exists a synergistic reaction between CeO_2 and ZrO_2 in mesoporous $Ce_{0.67}Zr_{0.33}O_2$ contrasted with pure mesoporous CeO_2. Based on the literature,[9] an adjunction of Zr^{4+} into CeO_2's crystal lattice contributes to a significant increase in the reducibility of ceria ($Ce^{4+} \leftrightarrow Ce^{3+}$). Because Zr^{4+} incorporation results in the increase of oxygen vacancy generation and via oxygen vacancy generation, surface lattice oxygen promotes the reduction of Ce^{4+} to Ce^{3+}.[38] As is well-known, the surface oxygen acts as the most active oxygen and plays an indispensable role in NH_3-SCR reaction.[37] Based on XPS results, the surface oxygen content in mesoporous $Ce_{0.67}Zr_{0.33}O_2$ is much higher than that in mesoporous CeO_2 due to the interaction between the zirconium and cerium oxides. In summary, Zr^{4+} incorporation into CeO_2 brings about more oxygen vacancy generation so that accelerates the NH_3-SCR process.

<H1>4. Conclusions

A series of highly ordered mesoporous $Ce_xZr_{1-x}O_2$ with very good composite crystal structure, uniform size and large surface area were fabricated for NH_3-SCR of NO_X using KIT-6 as a hard template. The highly ordered mesoporous materials then characterized by TEM, XRD, BET, BJH, XPS, H_2-TPR, NH_3-TPD and in-situ DRIFT. The optimal $Ce_{0.67}Zr_{0.33}O_2$ sample showed the near 100% NO_X conversion ratio at 325°C, as well as high H_2O/SO_2 durability and thermal stability under test conditions. Characterization results indicated that the addition of Zr content enhanced the thermal performance and redox ability of mesoporous $Ce_xZr_{1-x}O_2$, which were responsible for the excellent NH_3-SCR performance. Finally, a possible redox reaction mechanism with the mesoporous $Ce_xZr_{1-x}O_2$ was proposed. All of the features above were indicated that mesoporous $Ce_xZr_{1-x}O_2$ can be accepted as a possible NH_3-SCR catalytic candidate in the future.

Supporting Information

Materials used in the whole tests, TEM images of KIT-6, mesoporous $Ce_{0.75}Zr_{0.25}O_2$, $Ce_{0.5}Zr_{0.5}O_2$, $Ce_{0.33}Zr_{0.67}O_2$, $Ce_{0.25}Zr_{0.75}O_2$, CeO_2 and ZrO_2.

<ACK>Acknowledgements

The authors gratefully acknowledge the financial support of the national natural science foundation of China (Grant 21377061,81270041), Independent innovation fund of Tianjin University(2015XRG0020), Key Laboratory of Colloid and Interface Chemistry (Shandong University, Ministry of Education)(201401) and by Natural Science Foundation of Tianjin (Grant No. 13ZCZDSF00300, 15JCYBJC48400).

<REF>References

<BIBL>

[1] L. Chen, J. Li and M. Ge,;1; Environ. Sci. Technol. 44(2010)9590-9596.

[2] W. M. Chen, Y. P. Ma, Z. Qu, Q. H. Liu, W. J. Huang, X. F. Hu and N. Q. Yan,;1; Environ. Sci. Technol. 48(2014)12199-12205.

[3] F. Can, S. Berland, S. Royer, X. Courtois and D. Duprez,;1; ACS Catal. 3(2013)1120 1132.

[4] J. Shibata, K. Shimiz, A. Satsuma, T. Hattori, Appl. Catal.,;1; B 37(2002)197-204.

[5] M. Piacentini, M. Maciejewski and A. Baiker, Appl. Catal.,;1; B 60(2005)265-275.

[6] A. Flura, F. Can, X. Courtois, S. Royer and D. Duprez, Appl. Catal.,;1; B 126(2012)275-289.

[7] T. Zhang, J. Liu, D. X. Wang, Z. Zhao, Y. C. Wei, K. Cheng, G. Y. Jiang and A. Duan;1;, Appl. Catal., B 148(2014)520-531.

[8] Y. Peng, J. H. Li, X. Huang, X. Li, W. K. Su and X. X. Sun,;1; Environ. Sci. Technol. 48 (2014)4515-4520.

[9] A. Väliheikki, K. C. Petallidou, C. M. Kalamaras, T. Kolli, M. Huuhtanen, T. Maunula, R. L. Keiski and A. M. Efstathiou;1;, Appl. Catal., B 156(2014)72-83.

[10] D. H. Shang, W. Cai, W. Zhao, Y. F. Bu and Q. Zhong,;1; Catal. Lett. 144 (2014)538-544.

[11] C. E. Horia, H. Permanaa, K. Y. S. Nga, A. Brennerb, K. Morec, K. M. Rahmoellerd and D. Belton;1;, Appl. Catal., B 16(1998)105-117.

[12] S. P. Ding, F. D. Liu, X. Y. Shi, K. Liu, Z. H. Lian, L. J. Xie and H. He,;1; ACS Appl. Mater. Interfaces 7(2014)9497-9506.

[13] Z. C. Si, D. Weng, X. D. Wu, J. Yang, B. Wang,;1; Catal. Commun. 11(2010)1045-1048.

[14] M. Y. Qiu, S. H. Zhan, H. B. Yu, D. D. Zhu and S. Q. Wang,;1; Nanoscale 7 (2015)2568-2577.

[15] B. Zhi, H. Ding, D. M. Wang, Y. Cao, Y. Zhang, X. Wang, Y. L. Liu and Q. S. Huo,;1; J. Mater. Chem. A 2(2014)2374-2382.

[16] D. Y. Zhang, L. W. Zheng, Y. Ma, L. Y. Lei, Q. G. Li, Y. Li, H. M. Luo, H. X. Feng and Y. Hao,;1; ACS Appl. Mater. Interfaces 6(2014)2657-2665.

[17] L. Zhang, L. Y. Shi, L. Huang, J. P. Zhang, R. H. Gao and D. S. Zhang,;1; ACS Catal. 4 (2014)1753-1763.

[18] C. Fang, L. Y. Shi, H. R. Li, L. Huang, J. P. Zhang and D. S. Zhang,;1; RSC Adv. 6 (2016)78727-78736.

[19] C. Gunathilake and M. Jaroniec,;1; ACS Appl. Mater. Interfaces 6(2014)13069-13078.

[20] Y. Ren, Z. Ma and P. G. Bruce,;1; J. Mater. Chem. 22(2012)15121-15127.
[21] Q. F. Li, L. X. Zeng, J. C. Wang, D. P. Tang, B. Q. Liu, G. N. Chen, and M. D. Wei,;1; ACS Appl. Mater. Interfaces 3(2011)1366-1373.
[22] J. Rosen, G. S. Hutchings and F. Jiao,;1; J. Am. Chem. Soc. 135(2013)4516-452.
[23] E. J. W. Crossland, N. Noel, V. Sivaram, T. Leijtens, J. A. Webber and H. J. Snaith,;1; Nature 14(2013)215-219.
[24] D. Y. Zhang, L. W. Zheng, Y. Ma, L. Y. Lei, Q. L. Li, Y. Li, H. M. Luo, H. X. Feng and Y. Hao,;1; ACS Appl. Mater. Interfaces 6(2014)2657-2665.
[25] C. Wang, L. Sun, Q. Q. Cao, B. Q. Hu, Z. W. Huang and X. F. Tang, Appl. Catal.,;1; B 101(2011)598-605.
[26] P. F. Ji, J. L. Zhang, F. Chen and M. Anpo,;1; J. Phys. Chem. C 112(2008)17809-17813.
[27] C. M. Ho, J. C. Yu, T. Kwong, A. C. Mak and S. Lai,;1; Chem. Mater. 17(2005)4514-4522.
[28] Z. L. Li, R. Wnetrzak, W. Kwapinski and J. J. Leahy,;1; ACS Appl. Mater. Interfaces 4 (2012)4499-4505.
[29] C. C. Liu, S. Lee, D. Su, B. Lee, S. Lee, R. E. Winans, C. R. Yin, S. Vajda, L. Pfefferle and G. L. Haller,;1; Langmuir 28(2012)17159-17167.
[30] B. Zhi, H. Ding, D. M. Wang, Y. Cao, Y. Zhang, X. Wang, Y. L. Liu and Q. S. Huo,;1; J. Mater. Chem. A 2(2014)2374-2382.
[31] J. G. Deng, L. Zhang, H. X. Dai, Y. S. Xia, H. Y. Jiang, H. Zhang and H. He,;1; J. Phys. Chem. C 114(2010)2694-2700.
[32] Y. J. Sa, K. J. Kwon, J. Y. Cheon, F. Kleitzc and S. H. Joo,;1; J. Mater. Chem. A 1 (2013) 9992-10001.
[33] N. Jiang, J. Hu, J. Li, K. F. Shang, N. Lu and Y. Wu;1;, Appl. Catal., B 184(2016) 355-363.
[34] L. L. Zhang, J. J. Tu, L. Lyu and C. Hu;1;, Appl. Catal., B 181(2016)561-569.
[35] M. M. Antunes, S. Lima, P. Neves, A. L. Magalhães, E. Fazio, F. Neri, M. T. Pereira, A. F. Silva, C. M. Silva, S. M. Rocha, M. Pillinger, A.Urakawa and A. A. Valente;1;, Appl. Catal., B 182(2016)485-503.

[36] Y. Shu, H. Sun, X. Quan and S. Chen,;1; J. Phys. Chem. C 116(2012)25319-25327.

[37] D. S Zhang, L. Zhang, L. Y. Shi, C. Fang, H. R. Li, R. H. Gao, L. Huang and J. P. Zhang;1; Nanoscale 5(2013)1127-1136.

[38] J. Yu, Z. C. Si, L. Chen, X. D. Wu, D. Weng,;1; Appl. Catal., B 163(2015)223-232.

[39] S. X. Cai, D. S. Zhang, L. Zhang, L. Huang, H. R. Li, R. H. Gao, L. Y. Shi and J. P. Zhang,;1; Catal. Sci. Technol. 4(2014)93-101.

[40] Z. M. Liu, H. Su, J. H. Li and Y. Li,;1; Catal. Commun. 65(2015)51-54.

[41] X. Y. Wang, L. L. Jiang, J. Y. Wang and R. H. Wang,;1; Appl. Catal., B 165(2015)700-705.

[42] S. Letichevsky, C. A. Tellez, R.;1; R. d. Avillez, M. I. P. d. Silva, M. A. Fraga and L. G. Appel, Appl. Catal., B 58(2005)203-210.

[43] D. H. Shang, W. Cai, W. Zhao, Y. F. Bu and Q. Zhong,;1; Catal. Lett. 144(2014)538-544.

[44] L. Zhang, L. L. Li, Y. Cao, X. J. Yao, C. Y. Ge, F. Gao, Y. Deng, C. J. Tang and L. Dong;1;, Appl. Catal., B 165(2015)589-598.

[45] D. Wang, L. Zhang, K. Kamasamudram and W. S. Epling,;1; ACS Catal. 3(2013)871-881.

[46] H. Hu, S. X. Cai, H. R. Li, L. Huang, L. Y. Shi and D. S. Zhang,;1; ACS Catal. 5(2015) 6069-6077.

[47] X. Y. Zhang, Q. Shen, C. He, C. Y. Ma, J. Cheng, L. D. Li and Z. P. Hao,;1; ACS Catal. 2(2012)512-520.

[48] Z. M. Liu, S. X. Zhang, J. H. Li, J. Z. Zhu and L. L. Ma;1;, Appl. Catal., B 158 (2014)11-19.

</BIBL>
<Figure>Fig. 1 Schematic representation of the synthesis processes of mesoporous $Ce_xZr_{1-x}O_2$ with KIT-6.
<Figure>Fig. 2. NO_X conversion ratios of mesoporous $Ce_xZr_{1-x}O_2$ with different doped ratio (a), mesoporous/bulk $Ce_{0.67}Zr_{0.33}O_2$ and commercial VWTi (b), N_2 selectivity for mesoporous and bulk $Ce_{0.67}Zr_{0.33}O_2$ (b inset), mesoporous/bulk $Ce_{0.67}Zr_{0.33}O_2$ and commercial VWTi under different GHSVs (c-e). Conditions: 500 ppm NO, 500 ppm NH_3, 3% O_2, GHSV of 90000 h^{-1} (a, b) and N_2 balance gas.
<Figure>Fig. 3.TEM images of mesoporous (a) $Ce_{0.75}Zr_{0.25}O_2$ (a), (b) $Ce_{0.67}Zr_{0.33}O_2$, (c) bulk $Ce_{0.67}Zr_{0.33}O_2$, (d) CeO_2, HRTEM image of mesoporous (e) $Ce_{0.67}Zr_{0.33}O_2$ and the energy spectrum analysis (EDS) of mesoporous (f) $Ce_{0.67}Zr_{0.33}O_2$.
<Figure>Fig. 4. Low-angle XRD patterns (a) and wide-angle XRD patterns (b) of mesoporous $Ce_xZr_{1-x}O_2$.
<Figure>Fig. 5. (a-b) N_2 adsorption-desorption isotherms and (c-d) pore diameter distributions of mesoporous $Ce_XZr_{1-X}O_2$ and bulk $Ce_{0.67}Zr_{0.33}O_2$.
<Figure>Fig. 6. XPS spectrum of mesoporous $Ce_xZr_{1-x}O_2$ and bulk $Ce_{0.67}Zr_{0.33}O_2$, (a) Ce 3d, (b-c) Zr 3d, (d-e) O 1s, (f) wide-scan spectra.
<Figure>Fig. 7. H_2-TPR patterns (a-b), NH_3-TPD patterns (c-d) of mesoporous $Ce_xZr_{1-x}O_2$ and bulk $Ce_{0.67}Zr_{0.33}O_2$.

<Figure>Fig. 8. Raman spectra of mesoporous $Ce_xZr_{1-x}O_2$ and bulk $Ce_{0.67}Zr_{0.33}O_2$.
<Figure>Fig. 9. Tests of H_2O resistance (a, b), SO_2 resistance (c) and stability (d) over mesoporous $Ce_{0.67}Zr_{0.33}O_2$,V_2O_5-WO_3/TiO_2 and bulk $Ce_{0.67}Zr_{0.33}O_2$. Reaction conditions: reaction temperature at 300°C, [NO] = $[NH_3]$ = 500 ppm, $[O_2]$ = 5 vol %, $[H_2O]$ =10% or 15% while used, $[SO_2]$ = 100 ppm while used, N_2 balance and GHSV = 90000 h^{-1}.
<Figure>Fig. 10. In-situ DRIFT spectra of (a) NO + O_2 adsorption; (b) NH_3 adsorption; (c) NH_3 reacted with preadsorbed NO + O_2 species; (d) NO + O_2 reacted with preadsorbed NH_3 species at 300 °C on mesoporous $Ce_{0.67}Zr_{0.33}O_2$.
<Figure>Fig. 11. The reaction mechanism of NH_3-SCR on mesoporous $Ce_xZr_{1-x}O_2$.

Tables

<Table>Table 1. Summary of the textural parameters of the samples.

Materials	**Specific surface area (m^2/g)**	**Pore volume (cm^3/g)**
mesoporous $Ce_{0.75}Zr_{0.25}O_2$	118.8	0.34
mesoporous $Ce_{0.67}Zr_{0.33}O_2$	118.3	0.35
mesoporous $Ce_{0.5}Zr_{0.5}O_2$	110.1	0.29
mesoporous $Ce_{0.33}Zr_{0.67}O_2$	88.5	0.23
mesoporous $Ce_{0.25}Zr_{0.75}O_2$	79.4	0.22
mesoporous CeO_2	28.7	0.16
mesoporous ZrO_2	15.8	0.12
bulk $Ce_{0.67}Zr_{0.33}O_2$	68.9	0.21

<Table>Table 2. XPS analysis results of mesoporous $Ce_xZr_{1-x}O_2$ and bulk $Ce_{0.67}Zr_{0.33}O_2$

Materials	**Surface Atomic Concentration (%)**				
	Ce	Zr	O_α	O_β	O_{total}
mesoporous $Ce_{0.75}Zr_{0.25}O_2$	9.37%	0.94%	52.53%	37.16%	89.69%
mesoporous $Ce_{0.67}Zr_{0.33}O_2$	8.95%	1.06%	52.63%	37.36%	89.99%
bulk $Ce_{0.67}Zr_{0.33}O_2$	8.91%	1.69%	40.40%	49.00%	89.40%
mesoporous $Ce_{0.5}Zr_{0.5}O_2$	8.56%	2.61%	47.45%	41.38%	88.83%
mesoporous $Ce_{0.33}Zr_{0.67}O_2$	7.44%	5.01%	45.24%	42.31%	87.55%
mesoporous $Ce_{0.25}Zr_{0.75}O_2$	6.71%	6.39%	41.02%	45.88%	86.90%
mesoporous CeO_2	14.51%	0	37.06%	48.43%	85.49%
mesoporous ZrO_2	0	15.35%	20.9%	63.75%	84.65%

TDENDOFDOCTD